Heliyon 11 (2025) e42617

Contents lists available at ScienceDirect

Heliyon

journal homepage: www.cell.com/heliyon

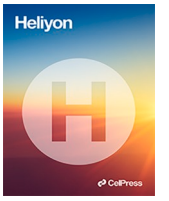

Research article

Social vulnerability: A driving force in amplifying the overall vulnerability of protected areas to natural hazards

Saied Pirasteh [a,b,1], Davood Mafi-Gholami [c,d,1], Huxiong Li [a,*], Tao Wang [a], Eric K. Zenner [e], Akram Nouri-Kamari [f], Tim G. Frazier [g], Saman Ghaffarian [h]

[a] Institute of Artificial Intelligence, Shaoxing University, 508 West Huancheng Road, Yuecheng District, Shaoxing,Zhejiang Province, 312000, China
[b] Department of Geotechnics and Geomatics, Saveetha School of Engineering, Saveetha Institute of Medical and Technical Sciences, Chennai, Tamilnadu, India
[c] Department of Forest Sciences, Faculty of Natural Resources and Earth Sciences, Shahrekord University, Shahrekord, 8818634141, Iran
[d] Metrology Research Group, Quality Assessment and Management Systems Research Center, Standard Research Institute, PO Box 31585-163, Alborz, Karaj, Iran
[e] Department of Ecosystem Science and Management, The Pennsylvania State University, Forest Resources Building, University Park, PA, 16802, USA
[f] Department of Geography Education, Farhangian University, Tehran, Iran
[g] Emergency and Disaster Management Program, School of Continuing Studies (SCS), Georgetown University, Washington, DC, USA
[h] Institute for Risk and Disaster Reduction, University College London, UK

ARTICLE INFO

Keywords:
FAHP
Spatial pattern
Integrated social-ecological framework and vulnerability assessment
Protected area management
Environmental hazard resilience

ABSTRACT

Incorporating social vulnerability (SoV) into vulnerability assessments for protected areas provides critical insights for enhancing the resilience and adaptability of these regions to environmental hazards. This study aimed to develop and apply an integrated social-ecological vulnerability assessment framework for a forest-protected area, focusing on scales relevant to management decisions. We collected data from 70 villages within the protected area through structured surveys, interviews, and reviews of secondary socio-economic and environmental datasets. A total of 24 socio-economic and environmental indicators were selected, based on expert consultation and literature review, to quantify the indices of exposure, sensitivity, adaptive capacity, and SoV. These indicators were weighted using the Fuzzy Analytical Hierarchy Process (FAHP) to ensure objective and expert-driven prioritization. Subsequently, the SoV index, derived from socio-economic metrics, was incorporated as a key variable in the exposure assessment. This integration involved 18 additional ecological indicators measured across a spatial grid, enabling a fine-scale analysis of the protected area's exposure, sensitivity, adaptive capacity, and overall vulnerability. Integrating social and ecological dimensions allowed for a spatially explicit evaluation of vulnerability at the grid-cell level, providing granular insights for localized management interventions. The results revealed that SoV significantly influenced the levels of exposure and overall vulnerability across the study area. High SoV values corresponded to areas with elevated overall vulnerability, emphasizing the interplay between social conditions and ecological risks. To enhance resilience in the medium and long term, the study recommends shifting investments

* Corresponding author.
E-mail addresses: sapirasteh1@usx.edu.cn (S. Pirasteh), d.mafigholami@sku.ac.ir (D. Mafi-Gholami), 2019000060@usx.edu.cn (H. Li), taohit@usx.edu.cn (T. Wang), eric.zenner@psu.edu (E.K. Zenner), a.nourikamari@cfu.ac.ir (A. Nouri-Kamari), Tim.Frazier@georgetown.edu (T.G. Frazier), s.ghaffarian@ucl.ac.uk (S. Ghaffarian).
[1] Equal contribution.

https://doi.org/10.1016/j.heliyon.2025.e42617
Received 29 December 2023; Received in revised form 7 February 2025; Accepted 10 February 2025
Available online 11 February 2025

toward active community engagement in conservation planning, increasing environmental awareness through education programs, and improving the socio-economic well-being of local communities to mitigate social vulnerability. This approach highlights the importance of integrating social dimensions into ecological assessments to inform more equitable and effective management strategies.

1. Introduction

Generally, the vulnerability conceptualization follows a social-ecological systems approach, assessing three dimensions: (a) Exposure, determined by environmental hazards like floods, droughts, landslides, wildfires, and climatic extremes. (b) Sensitivity is influenced by ecological conditions such as soil erosion, biomass change, and geological sensitivity, and (c) adaptive capacity is gauged by factors like water availability (runoff and spring discharge) and soil fertility. The framework integrates these dimensions spatially, using indices and a weighting system to evaluate the interplay between social and ecological factors [1–3]. The methodology emphasizes mapping and analyzing spatial variations to holistically understand the protected area's vulnerabilities, which will be explained in the methodology section.

Much like the larger environments into which they are embedded, protected areas (PA) are exposed to natural hazards such as wildfire, drought, increasing air temperature, and diseases, as well as continued human hazards resulting from exploitation, deforestation, conversion to agricultural lands, and pollutants and sewage deposition [4]. In rural areas where human communities are dependent on forest resources, forests and communities constitute a social-ecological system (with co-evolutionary relationships and mutual feedback) [5]. Activities of local communities such as agricultural expansion into the forest, deforestation, exploitation, illegal logging, collection of fuelwood and fodder, and deposition of pollutants and sewage are hazards that threaten and can even destroy forested PAs [4]. The intensity of hazardous activities is influenced by a set of characteristics of local rural communities that also determines the ability of the human communities to respond, cope or adjust to temporary and permanent stresses and changing conditions, thus influencing the level of social vulnerability/resilience of local communities to the same environmental hazards that threaten forested PAs. This often results in positive feedback whereby communities with a high degree of social vulnerability and precarious socio-economic conditions (low resilience) attempt to achieve lower sensitivity, greater adaptive capacity, and lower vulnerability through more intense exploitation of forest resources [6,7].

Spatially explicit vulnerability assessments of protected areas have been utilized in multiple studies to address vulnerabilities to various environmental hazards [8]. These assessments have not only identified vulnerable hotspots but have also enabled the prioritization of conservation efforts and informed targeted climate change adaptation planning, all in alignment with Sustainable Development Goal 13, also known as SDG-13 [9,10]. Except for one study [1], however, others either assessed the vulnerability of forested ecosystems without considering the social local subsystem [11–13] or assessed the vulnerabilities of the ecological and social subsystems separately and then combined the vulnerability of the subsystems [14]. However, due to the mutual feedback and co-evolutionary relations between the social and ecological subsystems, not considering one or separating both of these subsystems in the vulnerability assessment process may introduce bias, whereas combining separately assessed subsystem results may not accurately reflect the vulnerability of the entire system [1]. In fact, considering the social subsystem vulnerability as one of the factors of the exposure dimension of the ecological subsystem vulnerability directly incorporates mutual feedback between the two subsystems in the integrated vulnerability assessment process of systems. Furthermore, vulnerability assessments of forests typically use a limited set of sensitivity indicators related only to structural (e.g., extent and canopy cover) and functional features (e.g., production capacity, biomass above and below ground) and often omit broader biophysical indicators (i.e., physiographic, geological, hydrological, meteorological features) [9,15,16].

Nevertheless, the hypotheses and questions below address the identified gaps and provide a clear framework for analysis and testing, demonstrating the study's novelty and rationale for the above-mentioned studies. The hypothesis of this study comprises (a) incorporating SoV as an exposure variable in vulnerability assessments significantly influences the spatial distribution of overall vulnerability in the Helen Forest Reserve Area (HFPA). (b) The vulnerability of the social-ecological system exhibits spatial patterns correlated with the proximity of human communities and their socio-economic characteristics. (c) A broader set of biophysical indicators leads to a more comprehensive and accurate assessment of ecological vulnerabilities compared to using structural and functional indicators alone, and (d) Socio-economic challenges such as poverty and limited infrastructure access in local communities are positively correlated with higher ecological vulnerabilities in adjacent forest areas.

In this study, we consider a broad set of environmental, biophysical, and functional indicators of the sensitivity dimension and treat the vulnerability of the social subsystem as an important additional environmental hazard of the ecological subsystem of the Helen Forest Protected Area (hereafter 'HFPA') that is located in the Zagros Mountains in Iran [17]. Despite the high diversity of plant and animal species recorded in these forests and with about two million hectares in 52 protected areas (of which about 15 % are of international importance) [18], these forests continue to be exposed to natural and anthropogenic hazards such as drought, seismic activity, increasing air temperature, pests and diseases, and excessive livestock grazing, fuelwood and land use and land cover (LULC) changes [19–21]. As a consequence, significant declines in the richness and diversity of plant and animal species in recent years, as indicated by Asgari et al. [22], highlight the stress within the social-ecological system. It's probable that the challenging socio-economic conditions of local communities, characterized by poverty and limited access to infrastructure, play a contributing role in this phenomenon [10].

The objective of this study was to assess the vulnerability level of the social-ecological system of the HFPA and the local communities residing within the boundaries of the HFPA to environmental hazards. The contribution of this paper addresses the following critical questions: (1) How does integrating social vulnerability (SoV) as an exposure factor influence the overall vulnerability of the social-ecological system in the Helen Forest Protected Area (HFPA)? (2) What are the spatial patterns of vulnerability across the HFPA when considering both social and ecological subsystems together? To ass the vulnerability of the HFPA, we used the integrated framework developed by Mafi-Gholami et al. [1]. (3) Does incorporating a broader set of biophysical indicators significantly improve the accuracy of ecological vulnerability assessments in forested protected areas? (4) How do socio-economic conditions of local communities correlate with the spatial distribution of ecological vulnerabilities? Thus, the intent of assessing the vulnerability of the PAs is integrated, focusing on both social and ecological systems. The methodology evaluates how human activities and socio-economic conditions affect ecological resilience, aiming to balance conservation with community needs. This integrated approach helps understand the interdependencies and collective risks both systems face.

Finally, the rest of the paper includes a description of the study area, data and method used in this study. We provide a review of the literature in Section 2 to thoroughly show similar research. The methodology framework is explained in Section 3. The results of this study are presented in Section 4 and followed by a discussion in Section 5. Finally, we summarize the study in the conclusion section (Section 6).

2. Related works

Forests provide various ecological services and natural products and play an important role in ensuring human well-being at local, regional, and global scales [23]. For example, about 2 billion people in the world currently use forest wood products as a source of energy, and 54 % of all the wood harvested annually is used as fuel [24]. Further, non-timber forest products are frequently exploited to meet part of the livelihood needs of forest-dependent local communities worldwide [24]. The often-ensuing destruction of forests causes the loss of important resources and diminishes ecological services needed by the communities that depend most on them [23]. Forest destruction also releases huge amounts of carbon into the atmosphere, intensifying global warming, reducing surface and underground water quality, destroying habitats, and degrading biodiversity [4]. Thus, it is paramount to develop appropriate forest protection strategies to reduce the harmful effects of human activities on these ecosystems.

One strategy that aims to reverse the global loss of forests and biodiversity is establishing protected areas (PAs) [4,25]. Currently, PA networks cover nearly 15 % of the earth's surface area and are designed to restrict or mitigate anthropogenic pressures in areas of high biological diversity, such as forests [26,27]. PAs also provide vital ecosystem services and functions such as climate regulation, erosion control, groundwater recharge [16], and pollination [28].

The literature identifies vulnerability as a combination of three system dimensions: exposure, sensitivity, and adaptive capacity [29–31]. Exposure is the degree, duration, and extent to which a system is in contact with or is affected by disturbance [30]. Sensitivity is generally defined as the degree to which the system is affected or changed by exposure to one or a set of internal or external disturbances [32]. The adaptive capacity of a system includes the system's ability to cope with or adjust to potential damage and take advantage of opportunities to overcome the consequences of induced system changes [30]. This definition of vulnerability and its dimensions has inspired numerous integrated vulnerability assessments of coupled social-ecological systems to various hazards throughout the world, including in France [33], Mongolia [34], the UK [35], the United States [36,37], China [38], Brazil [39], Mexico [40], Australia [41,42] and Iran [1,43].

In regions such as mountainous areas, where both ecological and socio-economic systems face unique and intensified challenges, understanding vulnerability is essential. Such assessments aim to promote sustainable development by achieving a delicate balance between ecosystem preservation and socio-economic growth [44]. This goal is best pursued through the use of quantifiable indicators that allow for the separate evaluation of the vulnerability and resilience of different subsystems. These results are then synthesized into a composite index that is not only meaningful to decision-makers but also easily interpretable by the broader public [45,46], facilitating comparisons across diverse regions, including those with specific challenges like mountainous environments [1].

Mountainous regions are particularly vulnerable to a range of environmental hazards, including extreme weather events, erosion, landslides, and biodiversity loss, which are often compounded by the socio-economic dependence of local communities on fragile ecosystems. As such, these regions demand an integrated approach that takes into account both biophysical factors and human dynamics. Vulnerability in SESs arises from the intricate relationship between these environmental and socio-economic factors, underscoring the necessity for comprehensive, region-specific methodologies [47,48]. In this context, Yu et al. [49] emphasize the need for assessments beyond traditional ecological metrics by considering feedback loops and co-evolutionary interactions between the social and ecological subsystems. This approach is especially critical in mountainous areas, where the impact of environmental changes can be disproportionately high due to the sensitivity of these regions to climate variations. Recent studies, such as those by Gupta et al. [50], have highlighted the increasing significance of regional vulnerability assessments, particularly in high-altitude areas like the Indian Himalayas. These studies demonstrate the urgent need for adaptive strategies tailored to the specific vulnerabilities of mountainous regions.

Similarly, Das et al. [51] identified the role of spatial factors and social vulnerabilities in riparian zones along the Gangetic Plain, advocating for region-specific, spatially-informed adaptation measures. In Nainital, Chauhan et al. [52] emphasized the critical role of infrastructural and spatial indicators in assessing water vulnerability, underscoring the need for adaptive water management strategies in the face of fluctuating climate conditions. The studies discussed above underscore the critical importance of addressing the unique vulnerabilities of mountainous regions, which face distinct environmental and socio-economic challenges. These regions require targeted, context-specific approaches that consider both ecological and human factors in a comprehensive manner. By integrating both

dimensions, vulnerability assessments can more accurately capture the complexities of these areas and inform effective strategies for resilience. Such integrated assessments primarily aim to contribute to sustainable development by balancing ecosystem protection with socio-economic progress [44]. Achieving this objective involves the use of multiple measurable indicators that evaluate the vulnerability and resilience of various subsystems independently. These individual results are then combined into a composite index, which is not only accessible and understandable to both decision-makers and the public [46] but also enables meaningful comparisons across different regions. In mountainous areas, vulnerability assessments are especially critical due to the specific environmental pressures these regions face, such as rugged terrain, limited infrastructure, and increased exposure to natural hazards. Evaluating these vulnerabilities requires a thorough understanding of both the natural systems and the local communities that rely on them. As such, conducting these studies is vital for developing effective conservation strategies and adaptive measures that address the unique challenges of mountainous regions.

Ecological vulnerability assessments are crucial for understanding how ecosystems respond to natural and human-induced pressures, particularly in mountainous regions. Research by Bakkensen et al. [53], Rufat et al. [54], and Tellman et al. [55] underscores the importance of these assessments in shedding light on how ecosystems respond to climate change, land-use changes, and other environmental stressors. Additionally, historical data—discussed by Ong & Ellison [56], Kumar et al. [11], and Pokhriyal et al. [57]—provides vital insights into long-term ecological shifts, helping to assess the resilience and vulnerability of ecosystems over time. Integrating historical perspectives, as emphasized by Mafi-Gholami et al. [1], enriches the accuracy and reliability of vulnerability assessments, especially in mountain regions where historical patterns of land use and climate variations can inform current strategies.

Although there is no consensus or single framework for choosing indicators for assessing vulnerability [58,59], it is generally accepted that the scale and purpose of the study, as well as the availability and accuracy of data and information, should guide the selection process and be compatible with the temporal and spatial scales of management decisions [60]. Research indicates that indicators chosen to calculate the exposure index (EI) should relate to the frequency, intensity, or probability of occurrence of environmental hazards (e.g., occurrences of drought, flood, or maximum temperatures) [1,42,61]. The indicators used to calculate the sensitivity index (SI) should consider tolerance to changes caused by the occurrence of multiple environmental hazards (e.g., forest production potential or ecological variables of the landscape such as physiographic, soil or geological characteristics or social variables such as gender, education or income level) [9,36,61–64]. Indicators for the Adaptive Capacity Index (ACI) should relate to characteristics to overcome, adapt, or cope with environmental hazard impacts at minimal disruption (e.g., hydrological or edaphic characteristics of ecological subsystem or indicators such as employment and insurance status or access to infrastructure for the social subsystem) [1,9,62,63].

3. Material and methods

3.1. Study area

The Helen Forest Protected Area (HFPA), located in the Chaharmahal and Bakhtiari Province of southwestern Iran, spans 40,074 ha and forms part of the Zagros Mountains chain. The area lies at an elevation range of 1168 to 3225 m above sea level and is characterized by rugged mountainous topography. Positioned between latitudes 31°55′37″ to 32°00′08″ N and longitudes 50°53′11″ to 50°32′08″ E, HFPA represents a critical ecological zone with unique environmental and socio-economic dynamics (Fig. 1). The HFPA is predominantly covered by Iranian oak (Quercus persica), which accounts for approximately 75 % (28,595 ha) of the forest area [65]. This vegetation type supports a high level of biodiversity, particularly abundant bird species, contributing to the region's ecological

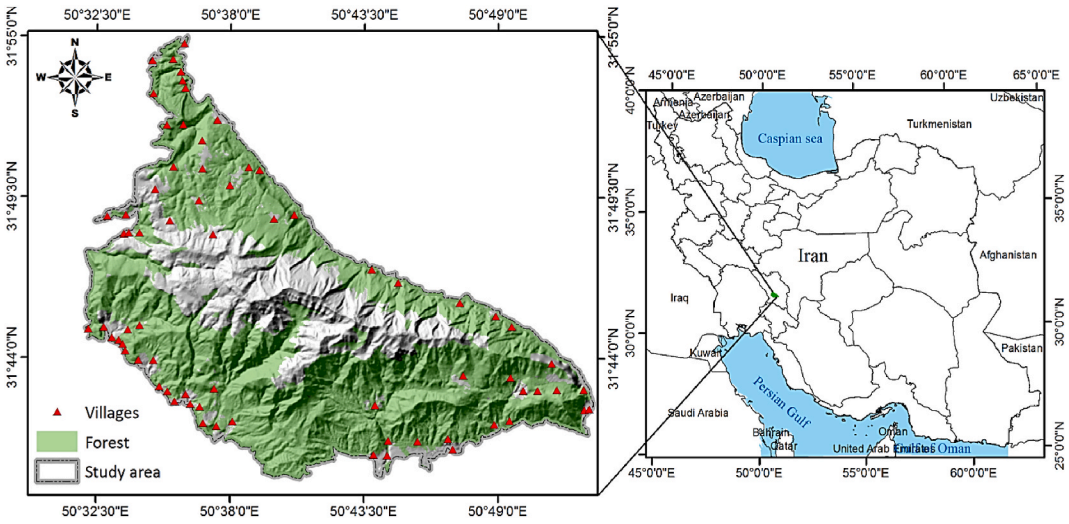

Fig. 1. Geographic location of the Helen Forest Protected Area in Iran.

significance. The dense oak forests provide essential ecosystem services, including soil stabilization, water retention, and habitat provision, while also serving as a buffer against environmental hazards.

The HFPA is home to 23,695 people living in 70 villages situated both within and around the protected area (https://www.amar.org.ir/english). Local communities are heavily dependent on the forest resources for their livelihoods. Key activities include livestock grazing, fuelwood and branch cutting, understory cultivation, and the intentional use of fire. While economically vital, these practices contribute to environmental degradation and pose significant risks to the forest's resilience. Additionally, hunting is a common activity affecting wildlife populations. The region experiences a semi-arid to Mediterranean climate, characterized by warm, dry summers and cold, wet winters. Precipitation is highly seasonal, often concentrated in the winter months, and is crucial for sustaining the vegetation and groundwater reserves. However, this climatic pattern also makes the area susceptible to droughts, further amplifying the pressure on forest resources and local livelihoods.

The soils in HFPA are predominantly shallow and rocky, typical of mountainous terrains, with variable fertility depending on elevation and vegetation cover. The presence of oak trees plays a vital role in preventing soil erosion by stabilizing the loose, fragmented terrain. However, human activities such as grazing and understory cultivation often disturb the soil, reducing water retention and fertility capacity. In addition to local exploitation, the HFPA faces external pressures from economic infrastructure developments, including the installation of oil pipelines, drinking water pipelines for villages, and high-voltage power transmission lines. These activities disrupt the ecological balance, threaten biodiversity, and exacerbate environmental hazards. The HFPA exemplifies the delicate interplay between ecological preservation and socio-economic demands. A nuanced understanding of vegetation, human dependence, climate, and soil dynamics is essential for developing effective conservation strategies that balance human needs with environmental sustainability.

3.2. Methodology framework and data sources

In this study, physiographic, climatic, geological, edaphic, hydrologic, socio-economic, and LULC data were collected from various sources such as the Plan and Budget Organization of Iran, the National Cartographic Center of Iran, the Iranian Meteorological Organization, the Iranian Census and Housing, the Forest, Range and Watershed Management Organization of Iran, and the Research Institute of Forests and Rangelands. The ecological parameters in the study form the environmental context for the vulnerability assessment of the protected area, and it includes (a) physiographic: elevation, slope, and aspect, (b) climatic: actual evapotranspiration (AET), drought magnitude, and maximum temperature changes, (c) geological: sensitivity of geological formations to erosion, (d) edaphic (soil-related): soil erosion and soil sensitivity to erosion, (e) hydrologic: runoff and spring discharge, (f) vegetative: biomass change over 20 years, and (g) LULC, which includes forest, range, shrub land, cultivation land, built-up, and bare land.

Additional data were obtained from a field survey of tree crown diameters, which, combined with analysis of Landsat 8 satellite images (downloaded from https://earthexplorer.usgs.gov/), was used to prepare the biomass map of the forests of the study area (Supplemental Fig. 1). Maps of landslides (Ngo et al., 2021), floods [66], earthquakes [67] and wildfires [68] were also used to compute the exposure index. The following flowchart methodology framework shows the vulnerability components used to implement the integrated vulnerability assessment process for the coupled social-ecological system of the HFPA (Fig. 2).

A review of previous studies on the vulnerability assessment of social-ecological systems, along with the frameworks developed in these studies [1,49,50], informed the integrated vulnerability assessment of the coupled social-ecological system of the HFPA. This assessment was conducted by combining the indices of exposure, sensitivity, and adaptive capacity through 11 distinct steps, outlined as follows.

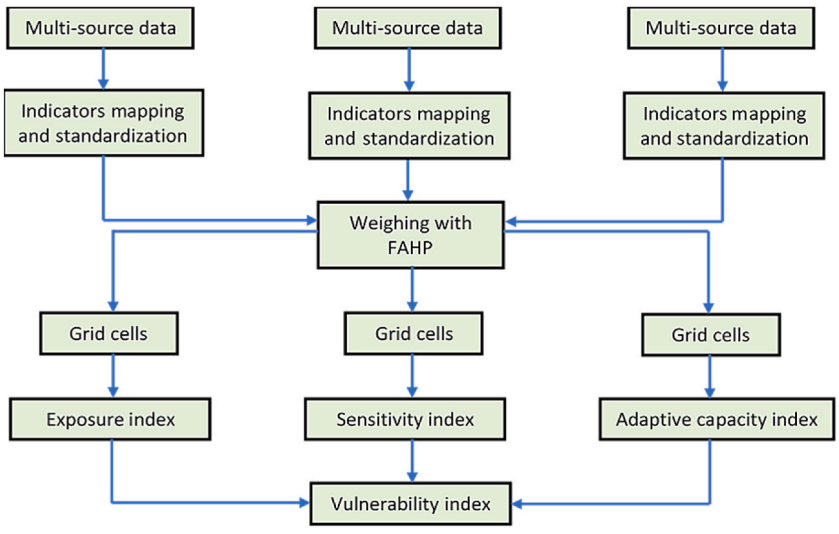

Fig. 2. The proposed process flowchart of the Helen Forest Protected Area vulnerability assessment framework.

1) Calculate and classify (standardization) multiple environmental hazard maps, including actual evapotranspiration, soil erosion, flood, extreme temperature, landslide, drought magnitude, wildfire and social vulnerability (SoVI) for the exposure dimension of the protected area.
2) Calculate and classify (standardization) height, slope, aspect, soil sensitivity to erosion, biomass change, geological formations sensitivity to erosion, average annual precipitation and LULC for the sensitivity dimension of the protected area.
3) Calculate and classify (standardization) runoff, LULC, spring discharge and soil fertility for the adaptive capacity dimension of the protected area.
4) Collect expert opinions and use the fuzzy analytical hierarchy process (FAHP) to calculate the relative weight of the variables (maps) of the exposure, sensitivity and adaptive capacity dimensions.
5) Multiply the relative weight of each variable in its standardized map and prepare a weighted map for all variables related to the exposure, sensitivity and adaptive capacity dimensions.
6) Combine the weighted maps of the variables and calculate the maps of the protected area's exposure, sensitivity and adaptive capacity dimensions.
7) Calculate the values of the exposure, sensitivity and adaptive capacity indices' values in each grid cell.
8) Combine the exposure, sensitivity and adaptive capacity indices in each of the grid cells and calculate the vulnerability index for all cells throughout the protected area.
9) Map spatial changes of vulnerability and its dimensions across the protected area.
10) Analyze the relationship between vulnerability and its dimensions and their indicators.
11) Analyze the spatial pattern of vulnerability across the protected area.

Table 1
Overview of dimensions and indicators of vulnerability assessment of the HFPA.

Dimension	Indicator	Description	Linkage	Scale	Source
Exposure	Drought magnitude	Assessment of drought severity	Influence on water availability and the structure and function of ecosystems	30 m	IMO [70]
	Extreme temperature	Frequency and intensity of extreme temperatures	Influence on ecosystem health and the growth, survival and composition of plant species	30 m	IMO [70]
	AET (mm)	Measurement of water loss from soil and plants	Influence on water availability and vegetation's structure and production potential	30 m	IMO [70]
	Social vulnerability	Measurement of community vulnerability to environmental hazards	Influence on disaster preparedness, recovery	30 m	ICC [71]
	Landslide	Probability of landslide occurrence	Influence on infrastructures, human settlements	30 m	Ngo et al. (2021)
	Flood	Probability of flood occurrence	Influence on infrastructures, human settlements, agriculture and ecosystems	30 m	Khosravi et al. [66]
	Soil erosion	Intensity of soil erosion	Impact on sedimentation, water quality and vegetation cover, infrastructures and human settlements	1:50000	NCCI [72]
	Wildfire	Probability of wildfire occurrence	Influence on vegetation infrastructures and human settlements	30 m	Jaafari et al. [68]
Sensitivity	Elevation (m)	Measurement of altitude above sea level	Influence on climate and ecosystem structure	30 m	DEM
	Slope (%)	Measurement of land inclination	Influence on erosion, vegetation cover and landslide susceptibility	30 m	DEM
	Aspect	Direction a slope faces relative to the sun	Influence on microclimate and vegetation cover	30 m	DEM
	Total biomass change (t ha^{-1})	Measures the variation in the overall biomass	impacts on ecosystem stability and vulnerability.	30 m	Satellite images
	Soil sensitivity to erosion	Susceptibility of soil to erosion	Impact on sedimentation, water quality and vegetation cover	1:50000	NCCI [72]
	Geological formations' sensitivity to erosion	Susceptibility of geological formations to erosion	Influence on landscape stability	1:50000	NCCI [72]
	Climate	Variation in precipitation and temperature over time	Influence on the structure and function of ecosystems, infrastructures, human health and agriculture	1:25000	IMO [70]
	LULC	Categorization of land cover types (e.g., forest, urban)	Influence on biodiversity, ecosystem services, habitat loss and fragmentation	1:50000	NCCI[72]
Adaptive capacity	Runoff (MCM)	The volume of water flowing over land	Influence on water availability and the structure and function of ecosystems	30 m	NCCI [72]
	Spring discharge (LS^{-1})	Flow of water from natural springs	Influence on water availability and the structure and function of ecosystems	30 m	NCCI [72]

Note: The National Cartographic Center of Iran (NCCI), the Plan and Budget Organization of Iran (PBOI), the Forest, Range and Watershed Management Organization of Iran (FRWMOI), the Iranian Meteorological Organization (IMO), the Iranian Census Centre (ICC), and the Research Institute of Forests and Rangelands (RIFR), Digital Elevation Model (DEM).

3.3. Indicators of vulnerability assessment

Previous assessments of the vulnerability of social-ecological systems in different regions were used to guide variable selection [11,12,14,69]. Further, physiographic, climatic, vegetative, geologic, edaphic, hydrologic and socio-economic data reflecting multiple environmental hazards were used to compute 42 variables (indicators) that capture the three dimensions of vulnerability of the HFPA. In addition, generally, the selection of indicators is based on.

(a) Relevance to the vulnerability dimensions (exposure, sensitivity, and adaptive capacity): Indicators directly capture environmental hazards, ecological sensitivities, and resilience capacities.
(b) Guidance from previous studies: Builds on established frameworks for social-ecological vulnerability assessment.
(c) Data availability: Relies on accessible and measurable data from diverse national and regional organizations.
(d) Expert input and local validation: Incorporates FAHP to weight variables based on expert opinions.
(e) Spatial representation: Variables were selected for their ability to capture spatial variations critical for mapping vulnerability.

Nevertheless, in this methodology, we describe the use of 42 indicators (variables) to evaluate the vulnerability dimensions (exposure, sensitivity, and adaptive capacity) of the HFPA. For example, this includes physiographic, climatic, vegetative, geologic, edaphic, hydrologic and socio-economic data that reflect multiple environmental hazards, and they were used to compute variables (indicators) that capture the three dimensions of the vulnerability of the HFPA (Table 1).

3.4. Calculation of the exposure index (EI)

The Exposure Index (EI) encapsulates the vulnerability of the Helen Forest Protected Area (HFPA) to environmental and social hazards. It integrates multiple standardized hazard indicators, such as actual evapotranspiration, drought magnitude, maximum temperature changes, floods, landslides, wildfire risks, soil erosion, and social vulnerability. These indicators are weighted using an FAHP based on expert inputs. Individual hazard maps are combined into a weighted EI map, capturing spatial variations in exposure across HFPA. High EI values indicate areas prone to compounded risks, which are essential for identifying hotspots of vulnerability and prioritizing interventions to enhance resilience and ecosystem stability. The following sections explain EI calculations in detail.

3.4.1. Actual evapotranspiration (AET)

This study obtained the required data from four synoptic stations around the protected area, including minimum and maximum monthly temperatures, wind speed at 2 m height, relative humidity, number of sunny hours per month, altitude, and geographic location. The data were entered into the CropWat software to compute annual PET values for each station for 2022. We used the empirical relationship to convert annual PET into AET at the watershed level [73] as Eq. (1):

$$\mathrm{AET} = \frac{\mathrm{P}}{\left(\alpha + \left(\frac{\mathrm{P}}{\mathrm{PET}}\right)^{\beta}\right)^{\frac{1}{\beta}}} \tag{1}$$

where $\alpha = 0.9$, $\beta = 2$, and P is annual rainfall. AET is the Actual Evapotranspiration (mm or other units of water depth). It represents the actual amount of water that is transferred from the land surface to the atmosphere through evaporation and plant transpiration. P denotes Precipitation (mm or other units of water depth). It is the total water input to the system from rainfall or other forms of precipitation. PET is the Potential Evapotranspiration (mm or other units of water depth). The maximum possible evapotranspiration that could occur under the prevailing atmospheric conditions, assuming unlimited water supply. A is the Model parameter (unitless or with dimensions depending on the formulation). A fitting parameter that accounts for the relationship between AET and precipitation under conditions of water surplus or deficit. It influences the shape of the curve relating AET and P, and finally, β is the Model parameter (unitless). It is a shape factor that determines the degree of nonlinearity between P, PET, and AET. Larger values of β make the relationship between P and AET more nonlinear.

3.4.2. Drought magnitude

To calculate the Standard Precipitation Index (SPI) value for each of the four synoptic stations situated across the HFPA, we utilized the 30-year time series (1990–2020) of monthly rainfall values recorded at these stations. Then, the drought magnitude over the 30-year period was computed for each station using equation (2) [1]:

$$\text{Drought Magnitude} = -\left(\sum_{j=1}^{x} SPI_j\right) \tag{2}$$

where SPI is the Standardized Precipitation Index, SPIj is the negative SPI value j running continuously over a period of x months.

3.4.3. Maximum temperature changes

We used long-term daily temperature data spanning a 37-year period (1986–2023) from the four synoptic climate stations to extract the maximum summer temperatures. We computed the average annual maximum summer temperatures and subsequently

utilized linear least-squares regression to establish a relationship between the mean maximum temperature values at each synoptic station and time. Then, the values of the rate of change of the mean maximum temperatures were computed and mapped throughout the HFPA using the IDW command in the ArcGIS 10.7 software.

3.4.4. Flood, landslide, wildfire, and soil erosion

The flood, landslide, and wildfire risk maps were based on spatial predictions of flood hazards in Iran [66], national scale landslide susceptibility maps of Iran, and wildfire occurrences in the Zagros eco-region [68]. The soil erosion map was obtained from the Ministry of Agriculture [74].

3.4.5. Social vulnerability of local communities

Communities with a higher degree of social vulnerability than others due to more precarious socio-economic characteristics typically respond with wider and more intense exploitation of forest resources that often imperil these ecosystems to achieve a higher level of adaptive capacity, a lower sensitivity, and a reduction of vulnerability [1,6]. We chose 24 indicators to evaluate the social vulnerability of local communities within the HFPA (Supplemental Table 1) [59,75]. In other words, we collected SoVI data from 24 socio-economic indicators that capture the social vulnerability of local communities in the study area. These indicators were selected based on prior studies and were evaluated using an FAHP, incorporating input from 12 experts and local residents. The indicators reflect socio-economic characteristics such as dependency on forest resources, economic resilience, and socio-demographic factors.

We employed the FAHP method to assess the importance of the indicators, relying on input from 12 experts and local residents. Subsequently, we calculated the relative weights of indicators. Following, weighted scores for each vulnerability dimension were determined by aggregating the weighted values of individual indicators. Considering that vulnerability has a negative relationship with adaptive capacity and a positive one with exposure and sensitivity, average social vulnerability index (SoVI) values for each village were computed as (Eq. (3)):

$$\mathrm{SoVI_i} = \frac{\left(\mathrm{DI_{Exposure_i}} + \mathrm{DI_{Sensitivity_i}}\right) - \left(\mathrm{DI_{Adaptive\ capacity_i}}\right)}{3} \tag{3}$$

where SoVI is the social vulnerability index for village i that can range between 0 and 1. DI is the Disaster Index, which is a numerical representation of each component (Exposure, Sensitivity, or Adaptive Capacity) based on specific indicators. Exposure_i is the degree to which the population or area is exposed to a hazard or disaster, such as floods, droughts, or extreme weather events in our study area. Sensitivity_i is the sensitivity of the population or area to the effects of the hazard, considering factors like socio-economic status, health, infrastructure, and other vulnerable characteristics. Adaptive Capacity_i is the ability of the population or area to adjust, cope, and recover from the impacts of the hazard. Higher adaptive capacity means better resilience to the hazard.

Villagers exploit the forest, let livestock graze, and directly influence the environment of the surrounding protected area up to a maximum distance of about 2.5 km distance around villages. In other words, we identified villages based on their proximity to the protected area, specifically their influence within a 2.5 km radius around the villages. The SoVI values for each village were computed using circular buffer zones extending outward in 50-m increments, creating an interpolated map of social vulnerability across the study area. Villages directly impacting the surrounding environment through activities like forest exploitation and livestock grazing were included in the analysis. The intensity of social vulnerability around each village was then computed for 50 concentric circular buffers

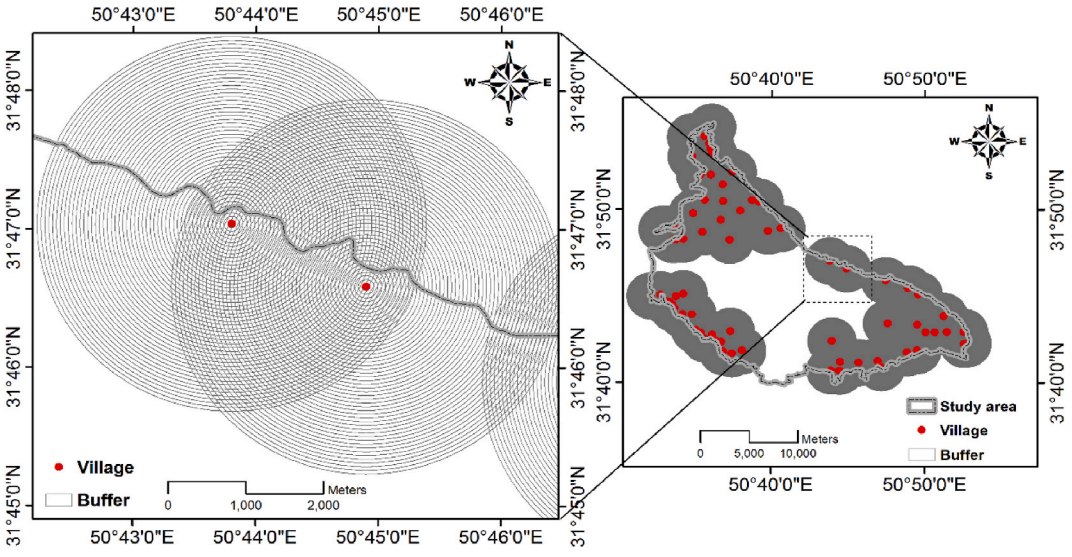

Fig. 3. Drawing concentric circular buffers that increased by a radius of 50 m around each village inside the Helen Forest Protected Area to compute social vulnerability intensity throughout the study area.

that increased by a radius of 50 m up to a total radius of 2500 m using the functions available in ArcGIS 10.7 software (Fig. 3) to create an interpolated SoVI map for the entire HFPA. Finally, the social vulnerability (LSoV) level was calculated in each 50 m wide circular buffer (see supplement for more details).

3.5. Calculation of the sensitivity index (SI)

Sensitivity analysis evaluates how input data or model parameter variations influence the vulnerability index. In this study, factors such as topographic elevation, slope, aspect, and soil erosion sensitivity are primary inputs for the sensitivity index. Their variability was modeled through classification and weighting techniques (e.g., FAHP), and maps were prepared to reflect standardized scores. By systematically varying input parameters (e.g., LULC reclassification thresholds or precipitation intensity classes), the robustness of the sensitivity index was tested. This process highlights which variables contribute most significantly to sensitivity, helping prioritize data collection or management actions. Incorporating error margins from classification, interpolation, or modeling ensures a realistic reflection of sensitivity trends and their impacts on vulnerability mapping. The following sections explain SI calculations in detail.

3.5.1. Elevation, aspect and slope

A topographic map with 20 m elevation curves was obtained from the National Geological Organization of the country [76] to make raster maps of elevation, aspect, and slope of the HFPA. The classification of the physiographic indicators maps was based on the principle that the vulnerability of the system increases by increasing the values of these indicators towards the threshold values [77, 78].

3.5.2. Soil and geological formations sensitivity to erosion

Maps of the sensitivity of the soil and geological formations to erosion were obtained from the National Geological Organization of the country (NGO, 2020).

3.5.3. Land use/land cover (LULC)

For this study, the LULC map of the HFPA included six classes (i.e., forest, range, scrub/shrub land, cultivation land, built-up area, and bare-land area) and was obtained from the General Department of Natural Resources and Watershed Management of the Chaharmahal and Bakhtiari Province [79]. LULC raster map was then re-classified into four categories that included Range and Forest (code 1), Scrub/shrub land (code 2), Cultivation land (code 3) and Built-up and Bare-land area (code 4).

3.5.4. Average annual precipitation

The map of the average annual rainfall across the HFPA was based on the average annual rainfall values spanning the 30-year time series between 1990 and 2020 of monthly rainfall data recorded at the four synoptic stations. Because increased amounts of rainfall and freshwater entering ecosystems reduce sensitivity and vulnerability to environmental hazards [57,80], very high values of annual rainfall in the classified map were indicated by the low category (code 1) and very low rainfall by the very high category (code 4). The average annual precipitation raster map was clipped using the vector map of the HFPA border and then classified into four categories.

Table 2
Threshold values of the four intensity classes for indicators of the three vulnerability dimensions in the HFPA.

Vulnerability dimension	Indicator	Intensity Category			
		Low (1)	Moderate (2)	High (3)	Very high (4)
Exposure	AET (mm)	<649.6	649.6–663.5	663.5–679.5	679.5<
	Drought magnitude	<108.5	108.5–109.8	109.8–110.9	110.9<
	LSoV	<0.365	0.365–0.635	0.635–0.819	0.819<
	Max. temperature (°C)	<0.026	0.026–0.034	0.034–0.044	0.044<
	Flood	<0.66	0.99–0.82	0.82–1.01	1.01<
	Landslide	<752	752–956	956–1068	1068<
	Fire	<0.35	0.35–0.59	0.59–0.82	0.82<
	Soil erosion	Low	Moderate	High	Very high
Sensitivity	Elevation (m)	<1656	1656–2057	2057–2493	2493<
	Slope (%)	<28	28–51	51–79	79<
	Aspect	Flat	South and west	North and east	No values
	TB change (t ha^{-1})	< −3.62	−3.62–−4.02	−4.02–−4.46	−4.46<
	Soil sensitivity to erosion	Low	Moderate	High	Very high
	Geological formations sensitivity to erosion	Low	Moderate	High	Very high
	Average annual precipitation (mm)	621<	561–621	498–561	<498
	LULC	Range and Forest	Scrub/shrub land	Cultivation land	Built-up and Bare-land area
Adaptive capacity	Runoff (MCM)	<38.57	38.57–44.20	44.20–48.87	48.87<
	Spring discharge (LS^{-1})	<39.15	39.15–44.10	44.10–48.79	48.79<

3.5.5. Total biomass change

Changes in total (above-plus below-ground) biomass of the HFPA were computed for the years between 2002 and 2022. For this purpose, by conducting the extensive field survey and estimating the values of the tree biomass in the sample plots, a regression relationship was established between the total biomass values of the sample plots and the Normalized Vegetation Difference Index (NDVI) value of four pixels corresponding in size to each sample plot [1,81]. The validated regression model was projected on the NDVI maps of 2022 and 2002 to enable computation of the total biomass of the protected area in these two years. For each raster map pixel, the total biomass of 2002 was subtracted from 2022 to show the total biomass change over 20 years across the entire HFPA (see supplement for more details).

3.6. Calculation of the adaptive capacity index (SI)

3.6.1. Runoff and spring discharge

Surface runoff and spring discharge volumes are indicators that determine the adaptive capacity of the HFPA. Data on surface runoff volumes of 23 sub-catchments and discharge values of 376 scattered springs throughout the HFPA were obtained from the General Department of Natural Resources and Watershed Management of Chaharmahal and Bakhtiari Province [79].

3.6.2. Raster maps and intensity classes of indicators

Raster maps of each indicator in individual 1000 m × 1000 m pixels were prepared in the ArcGIS 10.7 software covering the entire HFPA. Standardized indicator values were then classified into four classes (Table 2) using the ArcGIS 10.7 software: low (code 1), moderate (code 2), high (code 3) and very high (code 4).

3.6.3. Assigning weights to variables

To account for the different contributions of each indicator to the vulnerability of the HFPA [82–84], the FAHP method was used to evaluate the opinions of 12 experts on risk and vulnerability assessment, yielding relative weights for each indicator (see Ref. [1] for details). In this study, we selected 10 out of the 12 completed questionnaires based on a consistency ratio (CR) of less than 0.1 to establish indicator weights.

3.6.4. Calculation of EI, SI and ACI in the grid cells

The HFPA was divided into 469 grid cells with 1 km × 1 km (100 ha) dimensions to enable a spatially explicit vulnerability assessment of the social-ecological system. The size of the grid cells was equal to the minimum size of the management units used for strategic planning of environmental protection in protected areas in Iran. The standardized raster map of each indicator was multiplied with its relative weight derived from the FAHP. The index for each dimension was then computed as the sum of its respective indicators in each grid cell, and the calculation of the vulnerability index value was performed for each grid cell using Eq. (4) [1]:

$$VI = EI + SI - ACI \quad (4)$$

where VI is the Vulnerability Index, EI is the Exposure Index, SI is the Sensitivity Index, and ACI is the Adaptive Capacity Index.

In this study, the Natural Break command in ArcGIS 10.7 software was employed to explore the spatial patterns of vulnerability and

Table 3
The proportion of each of the variables of vulnerability dimensions in the HFPA.

Vulnerability dimension	Indicator	Category			
		Low (1) Area (%)	Moderate (2) Area (%)	High (3) Area %)	Very high (4) Area (%)
Exposure	AET (mm)	34.89	22.77	28.24	14.1
	Drought magnitude	15.16	33.68	31.82	19.34
	LSoV	13.35	19.46	20.54	14.19
	Maximum temperature	32.39	36.37	22.16	8.08
	Flood	20.5	41.62	23.75	14.13
	Landslide	0.62	27.90	46.40	25.08
	Wildfire	8.69	21.97	20.99	48.35
	Soil erosion	72.1	3.23	22.85	1.82
Sensitivity	Elevation (m)	23.30	31.31	24.88	20.50
	Slope (%)	27.78	35.98	27.55	8.7
	Aspect	0.80	49.40	49.80	–
	TB change (t ha^{-1})	11.18	28.18	24.26	7.74
	Soil sensitivity to erosion	2.74	65.31	30.22	1.74
	Geological formations' sensitivity to erosion	0.59	36.18	56.69	6.55
	Average Annual precipitation (mm)	29.46	30.01	26.95	13.58
	LULC	76.60	18.60	3.60	1.20
Adaptive capacity	Runoff (MCM)	7.83	33.29	33.14	25.74
	Spring discharge (LS^{-1})	13.58	26.95	30.01	29.46

its three dimensions in the grid cells across the HFPA. We assigned the index values in each grid cell into five categories, from very low to very high [85]. The relationship between vulnerability, its three dimensions, and their indices was examined using Pearson's r.

3.6.5. Spatial patterns of vulnerability in the protected area

This study used two spatial statistical methods, Global Moran's I (for spatial autocorrelation) and Anselin Local Moran's I (for cluster and outlier analysis), to investigate the spatial pattern of the Vulnerability Index (VI) throughout the HFPA. Global Moran's I coefficients were applied to analyze the spatial autocorrelation of VI values in grid cells [86]. Local Moran's I was utilized to discover spatial clusters in VI values across the HFPA [1]. This approach utilized the cluster/outlier patterns of High-High (HH), Low-Low (LL), High-Low (HL), and Low-High (LH) to map four typological gradations of vulnerability at the grid cell level. Hot spots (HH) and cold spots (LL) denote clusters of similar values and positive spatial autocorrelation, whereas LH and HL denote clusters of dissimilar values and negative spatial autocorrelation.

4. Results

4.1. Exposure factors

AET values increased from the eastern to the central parts and reached maximum values in the western parts of the HFPA (Supplemental Figs. 3 and 4); 42 % of the HFPA were in the high and very high AET categories (Table 3). Drought magnitude exhibited a strongly increasing north-to-south gradient (Supplemental Figs. 5 and 6); 51 % of the HFPA were in the high and very high drought intensity categories (Table 2). Maximum temperature changes increased along a north-to-south/southeast gradient (Supplemental Figs. 10 and 11); 30 % of the HFPA were in the high and very high categories (Table 3). A total of 38 % of the HFPA has high or very high flood risk, which was greatest along the entire outer perimeter and along rivers located in the western and southern portion of the area (Supplemental Figs. 12 and 13; Table 3). Similarly, landslide risks were greatest along the western and southern rivers as well as around most of the outer perimeter of the HFPA (Supplemental Figs. 14 and 15, Table 3). Wildfire risk showed a strong spatial pattern, with 69 % of the HFRA at high to very high risk, which was concentrated in the extreme north and along a wide margin along the western, southern, and south-eastern perimeter (Supplemental Figs. 16 and 17). About 25 % of the HFPA was classified as highly or very highly erodible. The central and southern portions of the HFPA had low soil erodibility (Table 3 and Supplemental Fig. 18).

Within the villages, the Social Vulnerability Index (SoVI) values varied from 0.32 to 0.90. The average SoVI value of 0.77 of the twenty western villages (29 %) was significantly different (both $P < 0.015$) from the average of 0.62 of the 27 northern villages (39 %) and the average of 0.61 of the 23 south-eastern villages (33 %) (Supplemental Fig. 7). This significant geographic difference in SoVI values was largely due to significantly greater exposure (both $P < 0.0025$) and sensitivity (both $P < 0.015$) in western villages compared to northern and southern/eastern villages. The level of social vulnerability (LSoV), which accounted for the overlapping spatial extent of effects of each village into its surrounding environment, brought the effective range of LSoV values of the portion of the HFPA located within 2.5 km of each village to between 0.016 and 1.484 (Supplemental Fig. 8), with largest spatial extents of high and very high LSoV values in the northern and western parts of the protected area (Supplemental Fig. 9).

4.2. Sensitivity factors

Elevation increased from the margins toward the center of the HFPA, with 23 % of the area in elevation class 1, 31 % in class 2, 25 % in class 3, and 21 % in class 4 (Table 3 and Supplemental Fig. 19). About 36 % of the HFPA was located on steep (51–79 % slope) and very steep (>79 %) slopes (Supplemental Fig. 20). Only 0.8 % of the HFPA was flat (class 1, no aspect), while southerly and westly aspects (49.4 %) and northly and eastly aspects (49.8 %) occupied similar extents (Table 3 and Supplemental Fig. 21). Aspect was mostly to the south and west in the nothern and eastern parts of the HFPA. Soil sensitivity to erosion showed a strong spatial pattern with high sensitivity along a band ranging from the northwest to the central part of the HFPA (Supplemental Fig. 22). Geological sensitivity to erosion was very high along a broad band ranging the width of the HFPA through the central part from its western to eastern margins (Supplemental Fig. 23); a total of 63 % had high or very high geological sensitivity to erosion. Based on the inverse relationship between the amount of rainfall and the degree of sensitivity to environmental hazards, 41 % of the area located in the eastern half of the HFPA was placed in the high and very high precipitation sensitivity classes (Table 3 and Supplemental Figs. 24 and 25). The classified LULC map showed that 76.6 % of the area was classified as Range and Forest (class 1), 18.6 % located in the centre as Scrub/Shrub land (class 2), 3.6 % located mostly along the western, southwestern and southern perimeter as Cultivation land (class 3), and 1.2 % as Built-up and Bare-land area (class 4) (Supplemental Fig. 26, Table 3).

The average diameter of tree crowns in the sample plots was 3.19 ± 0.14 m, which corresponds to average estimated AGB, BGB, and TB values of 25.08 ± 2.31 t/ha, 5.02 ± 0.42 t/ha, and 30.09 ± 2.86 t/ha, respectively, for the year 2022. Least squares regression

Table 4
Least squares regression (LSR) results for modeling the total biomass (TB) in the HFPA.

Variable	a	b	SE	Adj-r^2	P	N
TB (t/ha)	126.6963	1.413527	2.08	0.97	<0.001	80

a and b: slope and intercept of the regression equation.
SE: standard error of the equation.

showed a strong linear relationship between TB and NDVI values in the sample plots (coefficient of determination ($R^2 > 0.97$) (Table 4) whose validity was supported by the validation of the regression model using 30 % of sampling plots (35 plots) ($R^2 > 0.98$; $P < 0.001$).

Between 2002 and 2022, TB in forested areas based on the NDVI predictions decreased between −8.56 t/ha and −0.418 t/ha (Fig. 4), with 45 % of the forest area in high and very high biomass change classes that lost more than −4.02 t/ha (Table 3 and Fig. 5).

4.3. Adaptive capacity factors

Surface runoff volume in the sub-basins of the HFPA ranged from 34.6 MCM to 55.44 MCM, 59 % of mostly south-eastern and south-central parts of the HFPA in the high and very high runoff volume classes (Table 3 and Supplemental Figs. 27 and 28). Spring discharge values ranged from 35.25 L/S to 54.37 L/S, and 59 % were located in the western half of the HFPA in the high and very high discharge classes (Table 3 and Supplemental Figs. 30 and 31).

4.4. Relative weights of vulnerability indicators

Vulnerability assessment experts ranked (CR < 0.1) wildfire (0.98), drought (0.90), and social vulnerability (0.85) as the three most important exposure indicators; AET received the lowest relative weight (0.36) (Supplemental Fig. 32). Among the sensitivity indicators, total biomass change (0.98), soil sensitivity to erosion (0.95), and sensitivity of geological formations to erosion (0.86) occupied the top three ranks; however, aspect was ranked last (0.34) (Supplemental Fig. 33). Of the two indicators of adaptive capacity, spring discharge had a weight of 0.75 and runoff of 0.25.

4.5. Vulnerability index

4.5.1. Spatially explicit values of the vulnerability and its three dimensions indices across the protected area

About 28.8 % of the HFPA was in the high and very high exposure categories (Table 5), which were mostly concentrated in the northern and western portions of the area (Fig. 6). sensitivity was high or very high in 43.8 % of the area (Table 5), mostly in the central and south-eastern parts of the HFPA (Fig. 7). More than half of the area (57.7 %) was in the high and very high adaptive capacity categories (Table 5), which was concentrated in the western and northern parts of the HFPA (Fig. 8). More than one third (37.1 %) of the HFPA was designated to have high and very high overall vulnerability (Table 5) and was concentrated in the central and south-eastern parts of the HFPA; western and northern parts had mostly low and very low levels of vulnerability (Fig. 9).

4.5.2. Relationship of vulnerability to its three dimensions and their respective indicators

Significant correlations (all $p < 0.001$) were observed between the vulnerability index calculated for the grid cells and its three dimensions: sensitivity ($r = 0.89$), exposure ($r = 0.49$) and adaptive capacity ($r = -0.72$). (Supplemental Table 2). The indices of exposure, sensitivity and adaptive capacity dimensions were also correlated with their respective indicators. Exposure had the highest correlation with social vulnerability (LSoV) ($r = 0.63$) and the lowest correlation with drought ($r = 0.40$) (Supplemental Table 3). Sensitivity had the highest correlation with slope ($r = 0.62$) and the lowest correlation with total biomass changes ($r = 0.39$) (Supplemental Table 4). Adaptive capacity had the highest correlation with the spring discharges ($r = 0.83$) (Supplemental Table 5).

4.5.3. Spatial clustering of the vulnerability of grid cells across the protected area

Spatial autocorrelation analysis (Global Moran's I) of grid-cell vulnerability index values showed highly significant (z-score

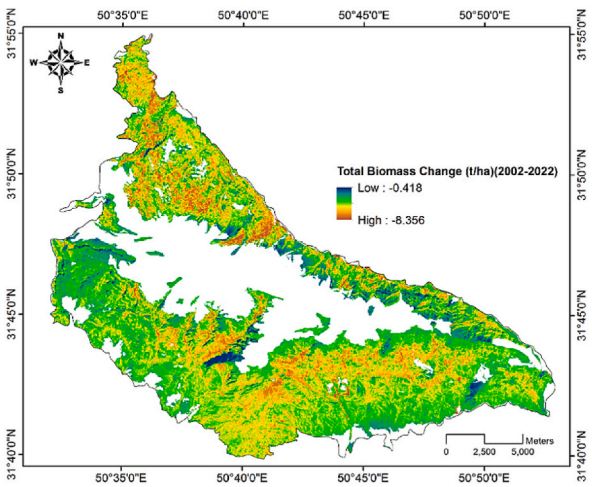

Fig. 4. Change in total biomass between 2002 and 2022 across the HFPA.

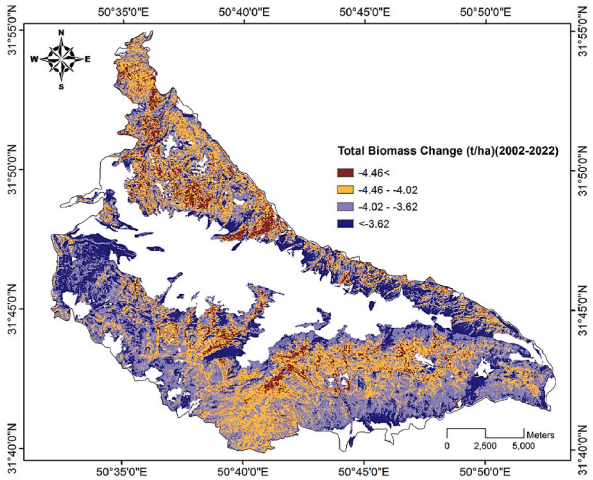

Fig. 5. Classification of total biomass change between 2002 and 2022 across the HFPA.

Table 5
The area (in % and in ha) in each of the five intensity classes of vulnerability and its three dimensions across the Helen Forest Protected Area. Total number of cells is 469.

Dimension	Category									
	Very low		Low		Moderate		High		Very high	
	Area (%)	Area (ha)	Area (%)	Area (ha)	Area (%)	Area (ha)	Area (%)	Area (ha)	Area (%)	Area (ha)
Exposure	13.0	5190.6	26.3	10550.2	31.9	12776.0	21.9	8792.8	6.9	2764.4
Sensitivity	6.3	2537.2	24.9	9961.1	25.0	10031.1	25.5	10218.5	18.3	7325.3
Adaptive capacity	13.4	5362.7	25.0	9997.7	3.9	1575.8	29.1	11652.5	28.7	11485.4
Vulnerability	16.7	6691.8	23.5	9419.7	22.7	9076.5	27.8	11157.2	9.3	3728.6

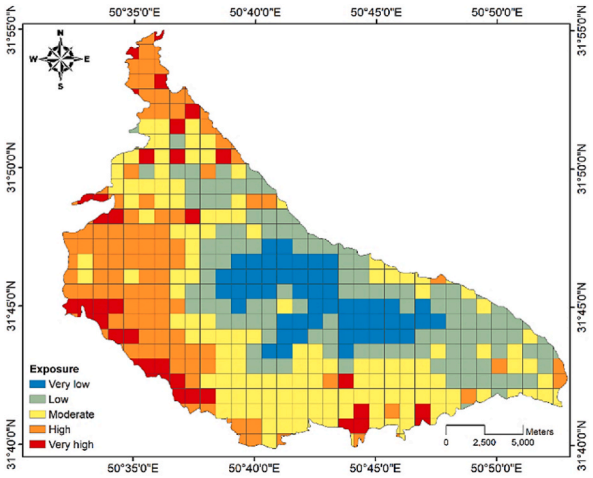

Fig. 6. Spatial pattern of exposure to multiple environmental hazards across the HFPA.

>19.62, $p < 0.001$) positive spatial correlations ($I = 0.68$) across the HFPA, meaning that neighboring grid cells exhibit similar vulnerability index values more often than expected by chance. Local Moran's I analysis showed 85 grid cells with high vulnerability index values (high-high) comprising a total area of 6957 ha (17.4 % of the total area); the largest cluster was located in the eastern part of the HFPA (Fig. 10). Clusters of cells with low vulnerability index values (low-low) comprised 80 grid cells and a total area of 7424 ha (18.5 %); the largest cluster was located in the northern part of the HFPA (Fig. 10).

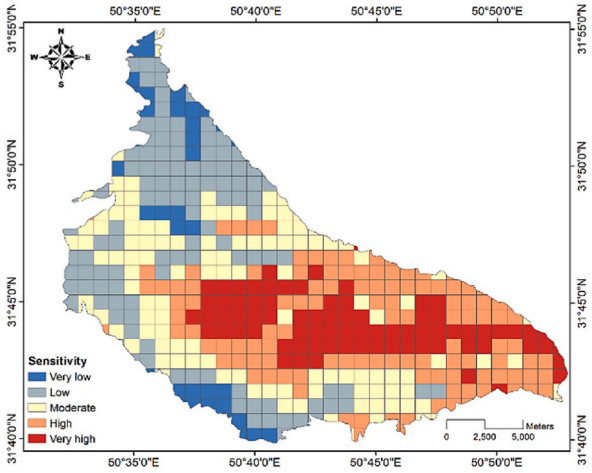

Fig. 7. Spatial pattern of sensitivity to multiple environmental hazards across the HFPA.

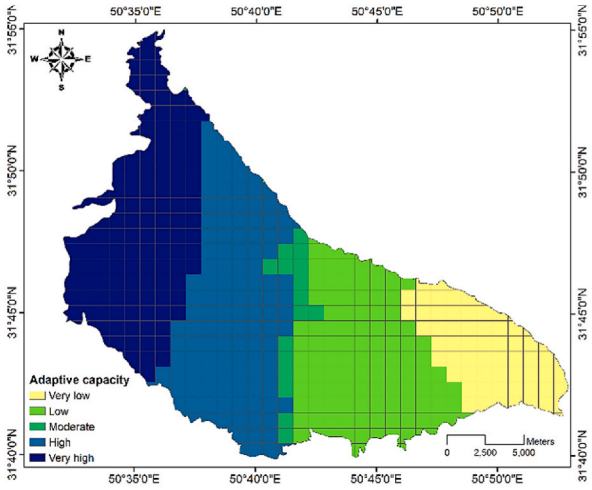

Fig. 8. Spatial pattern of adaptive capacity across the HFPA.

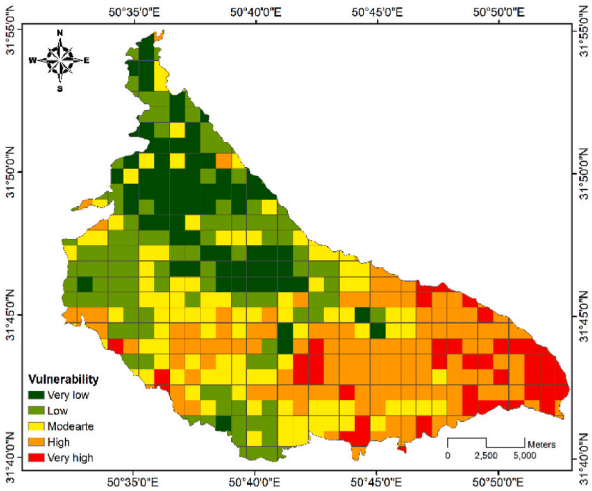

Fig. 9. Spatial pattern of vulnerability across the HFPA.

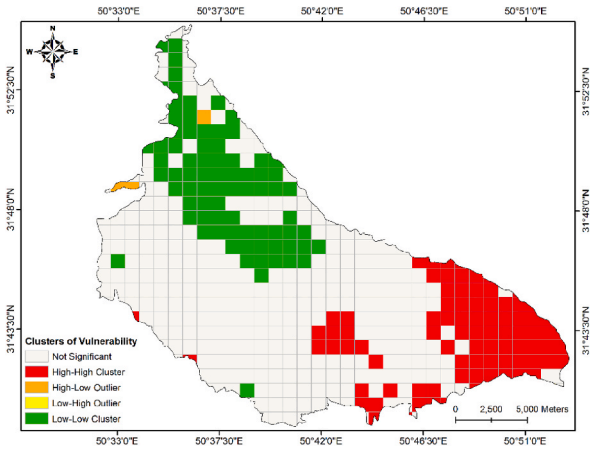

Fig. 10. Spatial clustering of grid cells based on the vulnerability similarity across the HFPA.

5. Discussion

The multiple environmental hazards to which the HFPA is exposed formed distinct individual spatial patterns and/or gradients throughout the protected area that either mirrored elevation (e.g., wildfire), topography (e.g., landslide) or the position of stream channels (e.g., flood), generally followed a north-south (e.g., drought, temperature) or an east-west intensity gradient (e.g., AET), or reflected the presence and influence of human habitation (e.g., social vulnerability). To better interpret the divergent spatial exposure patterns of the multiple environmental hazards, local expert opinion and the FAHP method were used to weigh the importance or priority of each hazard, which were then combined into a single compound exposure variable [1,83,84]. Similar to previous studies conducted in Zagros forests [10] and other socio-ecological systems [1,87], experts selected exposure to wildfire, drought, social vulnerability, and extreme summer temperatures as the greatest hazards affecting the structure and function in this forested ecosystem, exceeding the importance of soil erosion, flood, landslide, and annual evapotranspiration. When considering the weighted ensemble of environmental hazards, exposure exhibited strong spatial patterning across the HFPA, with high to very high levels of exposure in most of the western part and small portions of the extreme northern part of the HFPA. This spatial pattern did not closely resemble that of any hazard but was loosely coupled to flood, wildfire, landslide, and soil erosion risks across the landscape, which also exhibited the strongest correlations with this dimension. In comparison, local experts selected flood, drought, landslide, seismic activity, and extreme summer temperatures as the greatest hazards to which the villages residing within the HFPA are exposed. The set of hazard variables nonetheless resulted in an identical spatial exposure pattern for villages, with significantly greater exposure levels of villages located in the western part compared to those in the northern and southern/eastern part of the HFPA.

Local experts were acutely aware of the potentially destructive consequences of poor economic and social conditions of local communities residing within the HFPA when selecting the social vulnerability of villages as one of the most important environmental hazards in this study. Perhaps due to the greatest influence of this hazard in the periphery of the protected area, social vulnerability was slightly more strongly correlated with overall exposure than the other exposure indicators. The importance of this indicator is consistent with the documented high dependence of local communities on the Zagros forests for obtaining firewood and fuel, as well as fodder for livestock, which has caused irreparable damage to the integrity of these ecosystems [10]. Because local communities permanently use forests as a source of wood for livelihood or as animal feed [88], the economic well-being of communities breaks this dependence and seems to have an even greater impact on the rate of destruction of forest ecosystems than population size (Valiela et al., 2001).

Nonetheless, forest-dwelling communities' use of forest resources has been shown to reduce forest areas' production and production potential over time, and human activities may directly or indirectly change vegetation types [89]. It is thus not surprising that local experts saw change in forest biomass as the most important sensitivity variable that directly reflects the effects of environmental hazards on the production potential of this ecosystem [1,90], followed closely by the sensitivity of the soil and geological formations to erosion, average annual precipitation and LULC, and distantly by slope gradient, elevation, and aspect. Despite its importance, however, the influence of change in forest biomass on the compound sensitivity dimension was limited and exhibited the lowest correlation of all sensitivity indicators, which is likely due to the absence of forests at the highest elevations in the HFPA and the pervasive effects of climate change. The weighted ensemble of sensitivity indicators exhibited a strong spatial patterning across the HFPA that did not closely mirror the spatial pattern of any one indicator. Even so, high and very high sensitivity levels in the central to southern/eastern part of the HFPA were loosely coupled to steeper slopes and greater soil sensitivity to erosion in these areas as well as to an east-west gradient of average annual temperature that was also reflected by strongest correlations between these three indicators and the sensitivity dimension.

The adaptive capacity dimension in this study was a function of only surface runoff and spring discharge and exhibited a strong east-west gradient across the HFPA. The greatest adaptive capacity existed in the western part of the protected area, which received more precipitation and had greater amounts of surface runoff and spring discharge. The spatial pattern of the vulnerability index was

generally decoupled from that of exposure, largely mirrored that of sensitivity, and was weakly aligned with that of adaptive capacity, which was also reflected in the strength of the correlations of each dimension with vulnerability. Whereas high and very high exposure to environmental hazards was concentrated in the western and northern parts of the HFPA, high and very high sensitivity, low and very low adaptive capacity, and high and very high vulnerability were concentrated in the central and southern/eastern part of the protected area. In these areas, local Moran's I analysis showed significant spatial clustering of high levels of vulnerability in neighboring grid cells that covered nearly one-fifth of the total area of the HFPA, whereas significant clustering of low vulnerability was found on another one-fifth of the HFPA in the northern part.

Reducing the vulnerability of the HFPA would primarily benefit from a two-pronged management approach that seeks to reduce the sensitivity and increase the adaptive capacity of both the protected area itself and of communities residing within the protected area. However, management tools for reducing the sensitivity and increasing the adaptive capacity of the protected area are limited as no active forest management is permitted in the HFPA and measures are restricted to maintaining forest cover to prevent or mitigate soil erosion and (seasonal) flood occurrences, and strengthen aquifers in the HFPA [79] as well as building protection measures in villages with elevated flood and or landslide risks. In addition to limited managerial options that impact the forest directly, climate change-induced effects will likely increase exposure to more environmental hazards and negatively affect the protected area's sensitivity and adaptive capacity. It may thus be anticipated that predicted increases in the intensity of extreme rainfall events predicted for various regions of the world [91,92] will exacerbate flood events and associated severe soil erosion in steep areas that have high sensitivity of soil to erosion [93], which would likely be concentrated in the central and south-eastern parts and impact more than one-third of the HFPA.

Further, there is a predicted decrease in annual rainfall amounts and greater frequency occurrence of droughts caused by climate change in the coming decades in many parts of the globe [94] and especially in low latitudes and the Middle East [95] will further increase the sensitivity and vulnerability in some or all parts of HFPA). Indeed, the observed reduction in forest biomass in the HFRA over the last two decades is likely already the consequence of recent droughts [21,96], which, under the assumptions of the RCP 8.5 climate scenario are predicted to further increase in severity in the Chaharmahal and Bakhtiari Province in the coming decades [1,97]. In addition to adverse effects on the structure and function of the HFRA, predicted reductions in rainfall amounts and increased occurrences of drought will also reduce the volume of groundwater resources, spring discharge, and the volume of surface runoff, which will further increase the vulnerability of the protected area [98].

A more promising approach to reducing vulnerability might be to seek to reduce the sensitivity and increase the adaptive capacity of the human communities residing within the protected area. The spatial decoupling of social and ecological vulnerability, with high and very high social vulnerability predominantly in western villages and high and very high ecological vulnerability predominantly in southern villages, makes planning and resource allocation decisions very challenging. In the short term, investments in villages in the western part of the HFPA might seek to improve sensitivity and adaptive capacity's level. These villages generally have below-average income, level of education, and proportions of households living in their own home and above-average proportions of unemployed (economically inactive) people, uneducated population, disabled people, people over 64 years of age, and female-headed households, which may reflect greater livelihood dependence and thus greater use and destruction of adjacent forest areas. Thus, reducing livelihood dependence of local communities that adversely affect the HFPA might need to offer workshops for villagers and especially female-headed households to develop new sources of income through activities such as beekeeping, handicraft or carpet weaving production to create employment and supplement incomes.

Moreover, developing programs and educational workshops to increase local indigenous communities' awareness and knowledge of the environmental importance of the HFPA might also aid in preventing excessive exploitation and destruction of this protected area. In the medium and long term, investments may have to be shifted to communities that currently have lower social sensitivity and greater adaptive capacity but face greater exposure to hazards with climate change. For these communities, strengthening defensive measures against these hazards may become a top priority in a few years.

The vulnerability of socio-ecological systems in protected areas, such as the Helen Forest Protected Area (HFPA), is shaped by the interplay of ecological and social factors. Ecologically, climate change has intensified risks such as droughts, soil erosion, and habitat degradation, threatening the stability of ecosystems and the livelihoods dependent on them. These challenges are further exacerbated by human activities, including deforestation and unsustainable agricultural practices, which contribute to land degradation and biodiversity loss. Socially, limited access to resources, weak institutional support, and socio-economic disparities reduce the adaptive capacity of local communities, making them highly susceptible to environmental shocks and stressors. Addressing these interlinked vulnerabilities demands a comprehensive approach that integrates ecological and social dimensions into adaptive planning and management. Agroecological practices offer a promising pathway for enhancing resilience in protected areas. These practices focus on sustainable land use by promoting biodiversity, improving soil fertility, and ensuring food security. Indigenous agroforestry systems, for instance, integrate trees and shrubs into agricultural landscapes, providing multiple benefits such as carbon sequestration, erosion control, and supplementary income from non-timber forest products. Similarly, home gardens combine food production with biodiversity conservation and act as a socio-ecological buffer against economic and climatic risks. Such locally grounded strategies are particularly effective in contexts where traditional livelihoods are under threat from climate variability [99].

When practiced sustainably, shifting agriculture can also contribute to resilience by maintaining soil fertility and reducing pressure on vulnerable landscapes. This approach, coupled with community-driven water resources management, such as rainwater harvesting and efficient irrigation systems, addresses water scarcity and ensures agricultural productivity, particularly in arid and semi-arid regions [100]. These adaptive measures not only mitigate the impacts of climate change but also align with the broader goals of sustainable development. The role of indigenous knowledge systems in adaptation planning cannot be overstated. Traditional practices, such as the use of leguminous trees to enhance soil fertility and provide livestock feed during dry seasons, are highly effective in

mitigating climate-induced challenges. Indigenous knowledge also includes techniques for managing biodiversity, restoring degraded lands, and ensuring the sustainability of local resources. These practices have evolved over generations and are cost-effective and culturally relevant, making them essential components of any adaptation framework [99]. To build resilience, adopting an integrated management approach that prioritizes the interconnectedness of social and ecological systems is imperative. Community participation should be at the heart of this approach, ensuring local stakeholders have a voice in decision-making processes. Strengthening governance, enhancing education and capacity-building initiatives, and incentivizing sustainable land use are critical steps in fostering inclusive and effective adaptation. Moreover, aligning local adaptation strategies with international frameworks, such as the Sustainable Development Goals, can amplify their impact and provide access to global resources and expertise.

Finally, in this study, we identified synergies that are also found in adaptive capacity, particularly in areas with higher precipitation and runoff. However, climate change exacerbates risks, demanding strategies to mitigate impacts on both human and ecological systems. The results also highlight the spatially targeted investments. It addresses social vulnerability in western villages and ecological sensitivity in the southern regions and can balance immediate needs with long-term resilience. Therefore, the authors encourage sustainable PA management, which hinges on integrated approaches that align social equity with ecological conservation, ensuring mutual reinforcement rather than conflict.

6. Conclusion

This study delivers a comprehensive, spatially explicit vulnerability assessment of the Helen Forest Protected Area (HFPA), addressing climate change risks' intertwined social and ecological dimensions. By quantifying sensitivity, exposure, and adaptive capacity at scales relevant to both management and local communities, the findings provide actionable insights for adaptation planning. Through integrating expert opinions and the FAHP method, the study identified critical drivers of vulnerability, including wildfire, drought, soil erosion, and low adaptive capacity, enabling the identification of spatial hotspots for targeted interventions.

The outcomes of this study have practical implications for climate adaptation policies, particularly for protected areas and vulnerable communities. In the HFPA, distinct vulnerabilities call for tailored solutions. Villages in the western region, characterized by high social vulnerability and limited adaptive capacity, require immediate attention. Short-term measures should focus on improving education, healthcare, and livelihood diversification to reduce dependency on forest resources and enhance resilience. In the southern regions, where worsening drought conditions are projected, medium-to long-term strategies must emphasize sustainable water management, such as rainwater harvesting, watershed protection, and reforestation programs to mitigate erosion and maintain ecosystem health. Engaging local communities in participatory planning and education on the ecological significance of forests will be essential for fostering sustainable behaviors and long-term resilience.

Globally, this study offers a replicable framework for assessing vulnerability in protected areas. Recognizing the bidirectional relationships between social systems and ecological hazards highlights the need to integrate human and environmental dimensions in adaptation planning. The approach is particularly relevant for regions with similar socio-ecological dynamics, such as Sub-Saharan Africa or Southeast Asia, where forest-dependent communities face mounting climate risks. Policymakers and researchers can adapt this framework to identify vulnerabilities, prioritize interventions, and allocate resources effectively in other global contexts.

Despite its contributions, the study acknowledges several limitations. While valuable, reliance on expert judgment introduces subjectivity that could influence the weighting of indicators. Future assessments should integrate participatory approaches that incorporate local community insights to enhance objectivity. Additionally, the limited availability and resolution of spatial data constrained the detection of finer-scale variations in vulnerability. Future research should utilize higher-resolution datasets and advanced technologies such as Geospatial Artificial Intelligence (GeoAI) to enhance precision and identify micro-level vulnerabilities. Incorporating temporal dynamics to capture evolving climate impacts and expanding indicators to include socio-cultural and governance dimensions would further refine the robustness of vulnerability assessments.

The findings emphasize the importance of integrating vulnerability assessments into broader policy frameworks to guide resource allocation and adaptive management. Policymakers should leverage spatial vulnerability maps to design targeted, evidence-based adaptation strategies while fostering collaborations among researchers, local stakeholders, and governments to bridge the gap between science and policy.

Finally, this study provided critical insights for managing vulnerabilities in HFPA and serves as a model for advancing global adaptation efforts. Offering a transferable and integrative methodology contributes to the growing body of knowledge on climate resilience, paving the way for sustainable socio-ecological systems. In the face of escalating climate risks, such frameworks are indispensable for safeguarding ecosystems and the communities that depend on them.

CRediT authorship contribution statement

Saied Pirasteh: Writing – review & editing, Writing – original draft, Visualization, Validation, Supervision, Software, Resources, Project administration, Methodology, Investigation, Funding acquisition, Data curation, Conceptualization. **Davood Mafi-Gholami:** Writing – review & editing, Writing – original draft, Visualization, Validation, Software, Resources, Methodology, Formal analysis, Conceptualization. **Huxiong Li:** Visualization, Software, Resources, Project administration, Investigation, Funding acquisition. **Tao Wang:** Software, Resources, Investigation. **Eric K. Zenner:** Writing – review & editing, Software, Resources, Methodology, Formal analysis. **Akram Nouri-Kamari:** Software, Resources, Methodology, Investigation, Formal analysis, Data curation. **Tim G. Frazier:** Writing – review & editing, Software, Resources, Investigation, Formal analysis. **Saman Ghaffarian:** Validation, Software, Resources, Investigation.

Data availability

Data are available upon request. However, some data may be confidential and cannot be shared publicly.

Declaration of competing interest

The authors declare that they have no known competing financial interests or personal relationships that could have appeared to influence the work reported in this paper.

Acknowledgement

This work results from a joint research study between international collaborators to implement SDG-17. We thank all institutions that collaborated with their active participation in this research. This work was supported by the Natural Sciences Foundation of Zhejiang Province under Grant No. LY23F020006 and National Natural Science Foundation of China under Grant No. 62341208. We also appreciate the Institute of Artificial Intelligence, Shaoxing University, for collaboration and scientific support. This paper is supported by the Institute of Artificial Intelligence, Shaoxing University, under the project numbers 55–24002001003001/024 and 13011001002/244.

Appendix A. Supplementary data

Supplementary data to this article can be found online at https://doi.org/10.1016/j.heliyon.2025.e42617.

References

[1] D. Mafi-Gholami, S. Pirasteh, J.C. Ellison, A. Jaafari, Fuzzy-based vulnerability assessment of coupled social-ecological systems to multiple environmental hazards and climate change, J. Environ. Manag. 299 (2021) 113573.
[2] T. Wang, D. Mafi-Gholami, S. Pirasteh, X. Wang, H. Li, F. Chen, T.G. Frazier, A. Nouri-Kamari, A. Jaafari, A. Abulibdeh, Assessing spatial-temporal dynamics of vulnerability of protected areas in Iran to multiple environmental hazards, Int. J. Appl. Earth Obs. Geoinf. 132 (2024) 104053, https://doi.org/10.1016/j.jag.2024.104053.
[3] S. Pirasteh, Y. Fang, D. Mafi-Gholami, A. Abulibdeh, A. Nouri-Kamari, N. Khonsari, Enhancing vulnerability assessment through spatially explicit modeling of mountain social-ecological systems exposed to multiple environmental hazards, Sci. Total Environ. 630 (2024) 172744, https://doi.org/10.1016/j.scitotenv.2024.172744.
[4] R. Leberger, I.M. Rosa, C.A. Guerra, F. Wolf, H.M. Pereira, Global patterns of forest loss across IUCN categories of protected areas, Biol. Conserv. 241 (2020) 108299.
[5] D. González-Fernández, G. Hanke, M. Pogojeva, N. Machitadze, Y. Kotelnikova, et al., Floating marine macro litter in the Black Sea: toward baselines for large scale assessment, Environ. Pollut. 309 (2022) 119816, https://doi.org/10.1016/j.envpol.2022.119816.
[6] T.J. Timberlake, C.A. Schultz, Climate change vulnerability assessment for forest management: the case of the US Forest Service, Forests 10 (11) (2019) 1030.
[7] A. Sarkar, Minimalonomics: a novel economic model to address environmental sustainability and earth's carrying capacity, J. Clean. Prod. 371 (2022) 133663, https://doi.org/10.1016/j.jclepro.2022.133663.
[8] Ö. Ekmekcioğlu, K. Koc, Explainable step-wise binary classification for the susceptibility assessment of geo-hydrological hazards, Catena 216 (Part A) (2022) 106379, https://doi.org/10.1016/j.catena.2022.106379.
[9] J.S. Cao, Y.Q. Yang, Z.Y. Deng, Y.D. Hu, Spatial and temporal evolution of ecological vulnerability based on vulnerability scoring diagram model in Shennongjia, China, Sci. Rep. 12 (1) (2022) 5168.
[10] B. Mahmoudi, E. Zenner, D. Mafi-Gholami, F. Eshaghi, Livelihood analysis and a new inferential model for development of forest-dependent rural communities, Sustainability 15 (11) (2023) 9008.
[11] M. Kumar, N. Kalra, H. Singh, S. Sharma, P.S. Rawat, R.K. Singh, N.H. Ravindranath, Indicator-based vulnerability assessment of forest ecosystem in the Indian Western Himalayas: an analytical hierarchy process integrated approach, Ecol. Indic. 125 (2021) 107568.
[12] J. De Marco, L. Carturan, E. Maset, S. Cucchiaro, D. Visintini, R. De Infanti, F. Cazorzi, Century-long multi-source analyses highlight decreasing vulnerability for a small, debris-covered and avalanche-fed glacier in the eastern Italian Alps, J. Hydrol. 615 (2022) 128586.
[13] S. Kumi, P. Addo-Fordjour, B. Fei-Baffoe, Mining-induced changes in ecosystem services value and implications of their economic and relational cost in a mining landscape, Ghana, Heliyon 9 (10) (2023) e21156, https://doi.org/10.1016/j.heliyon.2023.e21156.
[14] N. Kanwar, J.C. Kuniyal, Vulnerability assessment of forest ecosystems focusing on climate change, hazards and anthropogenic pressures in the cold desert of Kinnaur district, northwestern Indian Himalaya, J. Earth Syst. Sci. 131 (1) (2022) 51.
[15] S.L. Powell, W.B. Cohen, S.P. Healey, R.E. Kennedy, G.G. Moisen, K.B. Pierce, J.L. Ohmann, Quantification of live aboveground forest biomass dynamics with Landsat time-series and field inventory data: a comparison of empirical modeling approaches, Rem. Sens. Environ. 114 (5) (2010) 1053–1068.
[16] X. Wei, G. Liu, Z. Rui, S. Pirasteh, W. Xiaowen, M. Wenfei, L. Song, X. Lingxiao, Modelling saline mudflat and aquifer deformation synthesizing environmental and hydrogeological factors using time-series InSAR, Journal of Selected Topics in Applied Earth Observations and Remote Sensing (2021), https://doi.org/10.1109/JSTARS.2021.3123514.
[17] D. Mafi-Gholami, J. Feghhi, A. Danehkar, N. Yarali, Prioritizing stresses and disturbances affecting mangrove forests using Fuzzy Analytic Hierarchy Process (FAHP). Case study: mangrove forests of Hormozgan Province, Iran, Advances in Environmental Sciences 7 (3) (2015) 442–459.
[18] S. Alemohammad, A.R. Yavari, B. Malek-Mohammadi, E. Salehi, M.J. Amiri, Landscape conservation and protected areas (case of Dena, Iran), Environ. Monit. Assess. 194 (2) (2022) 54.
[19] S. Pirasteh, K.P. Woodbridge, S.M. Rizvi, Geo-information technology (GiT) and tectonic signatures: the river Karun & dez, Zagros Orogen in south-west Iran, Int. J. Rem. Sens. 30 (1–2) (2009) 389–404.
[20] S. Pirasteh, S. Mollaee, S.N. Fatholahi, J. Li, Estimation of phytoplankton chlorophyll-a concentrations in the western basin of lake erie using sentinel-2 and sentinel-3 data, Can. J. Rem. Sens. (2020), https://doi.org/10.1080/07038992.2020.1823825.
[21] Q. Liu, C. Peng, R. Schneider, D. Cyr, N.G. McDowell, D. Kneeshaw, Drought-induced increase in tree mortality and corresponding decrease in the carbon sink capacity of Canada's boreal forests from 1970 to 2020, Glob. Change Biol. 29 (8) (2023) 2274–2285.

[22] Y. Asgari, M. Zobeiri, H. Sohrabi, Comparison of five distance sampling methods for estimating quantitative characteristics of Zagros Forests, Iranian Journal of Forest and Popular Research 21 (2) (2013) 316–328.
[23] R.P. Acharya, T. Maraseni, G. Cockfield, Global trend of forest ecosystem services valuation–An analysis of publications, Ecosyst. Serv. 39 (2019) 100979.
[24] FAO, Global Forest Resources Assessment 2020: Main Report, 2020. Rome.
[25] K.S. Andam, P.J. Ferraro, M.M. Hanauer, The effects of protected area systems on ecosystem restoration: a quasi-experimental design to estimate the impact of Costa Rica's protected area system on forest regrowth, Conservation Letters 6 (5) (2013) 317–323.
[26] O. Venter, R.A. Fuller, D.B. Segan, J. Carwardine, T. Brooks, S.H. Butchart, J.E. Watson, Targeting global protected area expansion for imperiled biodiversity, PLoS Biol. 12 (6) (2014) e1001891.
[27] J.E. Watson, E.S. Darling, O. Venter, M. Maron, J. Walston, H.P. Possingham, T.M. Brooks, Bolder science needed now for protected areas, Conserv. Biol. 30 (2) (2016) 243–248.
[28] L. Beaudrot, J.A. Ahumada, T. O'Brien, P. Alvarez-Loayza, K. Boekee, A. Campos-Arceiz, S.J. Andelman, Standardized assessment of biodiversity trends in tropical forest protected areas: the end is not in sight, PLoS Biol. 14 (1) (2016) e1002357.
[29] B.L. Turner, R.E. Kasperson, P.A. Matson, J.J. McCarthy, R.W. Corell, L. Christensen, A. Schiller, A framework for vulnerability analysis in sustainability science, Proc. Natl. Acad. Sci. USA 100 (14) (2003) 8074–8079.
[30] W.N. Adger, Vulnerability, Glob. Environ. Change 16 (3) (2006) 268–281.
[31] IPCC, in: S. Solomon, D. Qin, M. Manning, M. Marquis, K. Averyt (Eds.), Climate Change 2007: the Physical Science Basis: Contribution of Working Group I to the Fourth Assessment Report of the Intergovernmental Panel on Climate Change, H L Miller and Z Chen, 2007.
[32] G.C. Gallopín, Linkages between vulnerability, resilience, and adaptive capacity, Glob. Environ. Change 16 (3) (2006) 293–303.
[33] L. Thiault, S. Gelcich, N. Marshall, P. Marshall, F. Chlous, J. Claudet, Operationalizing vulnerability for social–ecological integration in conservation and natural resource management, Conservation Letters 13 (1) (2020) e12677.
[34] T. Chuluun, M. Altanbagana, D. Ojima, R. Tsolmon, B. Suvdantsetseg, Vulnerability of pastoral social-ecological systems in Mongolia. Rethinking Resilience, Adaptation and Transformation in a Time of Change, 2017, pp. 73–88.
[35] L.A. Naylor, U. Brady, T. Quinn, K. Brown, J.M. Anderies, A multiscale analysis of social-ecological system robustness and vulnerability in Cornwall, UK, Reg. Environ. Change 19 (2019) 1835–1848.
[36] S.L. Cutter, C.T. Emrich, D.P. Morath, C.M. Dunning, Integrating social vulnerability into federal flood risk management planning, Journal of Flood Risk Management 6 (4) (2013) 332–344.
[37] C. Armatas, T. Venn, A. Watson, Understanding social–ecological vulnerability with Q-methodology: a case study of water-based ecosystem services in Wyoming, USA, Sustain. Sci. 12 (2017) 105–121.
[38] X. Zhang, K. Liu, S. Wang, T. Wu, X. Li, J. Wang, Y. Ji, Spatiotemporal evolution of ecological vulnerability in the Yellow River Basin under ecological restoration initiatives, Ecol. Indic. 135 (2022) 108586.
[39] M. Hagenlocher, F.G. Renaud, S. Haas, Z. Sebesvari, Vulnerability and risk of deltaic social-ecological systems exposed to multiple hazards, Sci. Total Environ. 631 (2018) 71–80.
[40] A.P. Galicia-Gallardo, E. Ceccon, A. Castillo, C.E. González-Esquivel, An integrated assessment of social-ecological resilience in Me' phaa indigenous communities in southern Mexico, Hum. Ecol. 51 (1) (2023) 151–164.
[41] S.J. Metcalf, E.I. van Putten, S. Frusher, N.A. Marshall, M. Tull, N. Caputi, J. Shaw, Measuring the vulnerability of marine social-ecological systems: a prerequisite for the identification of climate change adaptations, Ecol. Soc. 20 (2) (2015).
[42] J.C. Ellison, Vulnerability assessment of mangroves to climate change and sea-level rise impacts, Wetl. Ecol. Manag. 23 (2015) 115–137.
[43] S. Pirasteh, E.K. Zenner, D. Mafi-Gholami, A. Jaafari, A.N. Kamari, G. Liu, J. Li, Modeling mangrove responses to multi-decadal climate change and anthropogenic impacts using a long-term time series of satellite imagery, Int. J. Appl. Earth Obs. Geoinf. 102 (2021) 102390.
[44] M.D.M. Delgado-Serrano, E. Oteros-Rozas, I. Ruiz-Mallén, D. Calvo-Boyero, C.E. Ortiz-Guerrero, R.I. Escalante-Semerena, E. Corbera, Influence of community-based natural resource management strategies in the resilience of social-ecological systems, Reg. Environ. Change 18 (2018) 581–592.
[45] J.E. Cinner, M.L. Barnes, Social dimensions of resilience in social-ecological systems, One Earth 1 (1) (2019) 51–56.
[46] D.S. Rickless, X.A. Yao, B. Orland, M. Welch-Devine, Assessing social vulnerability through a local lens: an integrated geovisual approach, Ann. Assoc. Am. Geogr. 110 (1) (2020) 36–55.
[47] S. Biswas, S. Nautiyal, A Review of Socio-Economic Vulnerability: the Emergence of its Theoretical Concepts, Models and Methodologies, Natural Hazards Research, 2023.
[48] O.V. Wilhelmi, R.E. Morss, Integrated analysis of societal vulnerability in an extreme precipitation event: a Fort Collins case study, Environ. Sci. Pol. 26 (2013) 49–62.
[49] X. Yu, Y. Li, M. Xi, F. Kong, M. Pang, Z. Yu, Ecological vulnerability analysis of beidagang national park, China, Front. Earth Sci. 13 (2019) 385–397.
[50] A.K. Gupta, M. Negi, S. Nandy, M. Kumar, V. Singh, D. Valente, R. Pandey, Mapping socio-environmental vulnerability to climate change in different altitude zones in the Indian Himalayas, Ecol. Indic. 109 (2020) 105787.
[51] M. Das, A. Das, S. Momin, R. Pandey, Mapping the effect of climate change on community livelihood vulnerability in the riparian region of Gangatic Plain, India, Ecol. Indic. 119 (2020) 106815.
[52] D. Chauhan, M. Thiyaharajan, A. Pandey, N. Singh, V. Singh, S. Sen, R. Pandey, Climate change water vulnerability and adaptation mechanism in a Himalayan City, Nainital, India, Environ. Sci. Pollut. Control Ser. (2021) 1–18.
[53] L.A. Bakkensen, C. Fox-Lent, L.K. Read, I. Linkov, Validating resilience and vulnerability indices in the context of natural disasters, Risk Anal. 37 (5) (2017) 982–1004.
[54] S. Rufat, E. Tate, C.T. Emrich, F. Antolini, How valid are social vulnerability models? Ann. Assoc. Am. Geogr. 109 (4) (2019) 1131–1153.
[55] B. Tellman, C. Schank, B. Schwarz, P.D. Howe, A. de Sherbinin, Using disaster outcomes to validate components of social vulnerability to floods: flood deaths and property damage across the USA, Sustainability 12 (15) (2020) 6006.
[56] W.J. Ong, J.C. Ellison, A framework for the quantitative assessment of mangrove resilience, in: Dynamic Sedimentary Environments of Mangrove Coasts, Elsevier, 2021, pp. 513–538.
[57] P. Pokhriyal, S. Rehman, G. Areendran, K. Raj, R. Pandey, M. Kumar, H. Sajjad, Assessing forest cover vulnerability in Uttarakhand, India using analytical hierarchy process, Modeling Earth Systems and Environment 6 (2020) 821–831.
[58] A. Asadzadeh, T. Kötter, E. Zebardast, An augmented approach for measurement of disaster resilience using connective factor analysis and analytic network process (F'ANP) model, Int. J. Disaster Risk Reduct. 14 (2015) 504–518.
[59] S. Su, J. Pi, C. Wan, H. Li, R. Xiao, B. Li, Categorizing social vulnerability patterns in Chinese coastal cities, Ocean Coast Manag. 116 (2015) 1–8.
[60] S.L. Cutter, S. Derakhshan, Implementing disaster policy: exploring scale and measurement schemes for disaster resilience, J. Homel. Secur. Emerg. Manag. 16 (3) (2019) 20180029.
[61] C. Jia, Y. Xinjun, Y. Sha, W. Kongsen, D. Mengqi, W. Xin, The vulnerability evolution and simulation of social-ecological systems in a semi-arid area: a case study of Yulin city, China, J. Geogr. Sci. 28 (2) (2018) 152–174.
[62] W. Wei, S. Shi, X. Zhang, L. Zhou, B. Xie, J. Zhou, C. Li, Regional-scale assessment of environmental vulnerability in an arid inland basin, Ecol. Indic. 109 (2020) 105792.
[63] D. Mafi-Gholami, E.K. Zenner, A. Jaafari, Mapping recent (1997–2017) and future (2030) county-level social vulnerability to socio-economic conditions and natural hazards throughout Iran, J. Clean. Prod. 355 (2022) 131841.
[64] B. Chisadza, F. Ncube, M. Macherera, T. Bangira, O. Gwate, Spatio-temporal variations in the ecological vulnerability of the Upper Mzingwane sub-catchment of Zimbabwe, Geomatics Nat. Hazards Risk 14 (1) (2023) 2190857.
[65] A. Moradi, N. Shabanian, Land-use change in the Zagros forests and its impact on soil carbon sequestration, Environ. Dev. Sustain. (2022) 1–16.

[66] K. Khosravi, M. Panahi, A. Golkarian, S.D. Keesstra, P.M. Saco, D.T. Bui, S. Lee, Convolutional neural network approach for spatial prediction of flood hazard at national scale of Iran, J. Hydrol. 591 (2020) 125552.
[67] H. Hamzehloo, A. Alikhanzadeh, M. Rahmani, A. Ansari, Seismic hazard maps of Iran, in: Proceedings of the 15th World Conference on Earthquake Engineering, 2012, pp. 24–28. Lisbon, Portugal.
[68] A. Jaafari, O. Rahmati, E.K. Zenner, D. Mafi-Gholami, Anthropogenic activities amplify wildfire occurrence in the Zagros eco-region of western Iran, Nat. Hazards 114 (1) (2022) 457–473.
[69] X. Tai, W. Xiao, Y. Tang, A quantitative assessment of vulnerability using social-economic-natural compound ecosystem framework in coal mining cities, J. Clean. Prod. 258 (2020) 120969.
[70] Iranian Meteorological Organization (IMO) (2023). https://www.irimo.ir/. (Accessed 5 June 2023).
[71] Iranian Census Centre (ICC) (2023). https://irandataportal.syr.edu/census. (Accessed 2 March 2023).
[72] National Cartographic Center of Iran (NCCI) (2023). https://ncc.gov.ir/. (Accessed 17 August 2023).
[73] K. Abdollahi, I. Bashir, B. Verbeiren, M.R. Harouna, A. Van Griensven, M. Huysmans, O. Batelaan, A distributed monthly water balance model: formulation and application on Black Volta Basin, Environ. Earth Sci. 76 (2017) 1–18.
[74] Ministry of Agriculture Jihad (MAJ), National Soil Quality Report, 2019, p. 250.
[75] S.L. Cutter, C. Finch, Temporal and spatial changes in social vulnerability to natural hazards, Proc. Natl. Acad. Sci. USA 105 (7) (2008) 2301–2306.
[76] National Geological Organization of Iran (NGO), The Report of Soil and Geology of the Country, 2022, p. 236.
[77] M.F. Makhdoum, Degradation model: a quantitative EIA instrument, acting as a Decision Support System (DSS) for environmental management, Environ. Manag. 30 (2002) 151–156.
[78] I. Shirmohammadi, A. Jahani, V. Etemad, N. Zargham, M. Makhdom, Development environmental impact assessment (EIA) on karkas protected area by using destruction, Environ. Res. 7 (14) (2017) 91–102.
[79] CHBNRWM: General Department of Natural Resources and Watershed Management of Chaharmahal and Bakhtiari Province, Watershed Management Plan and Cooperative Management of Forest Areas in Chaharmahal and Bakhtiari Province, 2023, p. 426.
[80] D. He, K. Hou, X.X. Li, S.Q. Wu, L.X. Ma, A reliable ecological vulnerability approach based on the construction of optimal evaluation systems and evolutionary tracking models, J. Clean. Prod. 419 (2023) 138246.
[81] T.W. Gillespie, S. Ostermann-Kelm, C. Dong, K.S. Willis, G.S. Okin, G.M. MacDonald, Monitoring changes of NDVI in protected areas of southern California, Ecol. Indic. 88 (2018) 485–494.
[82] J. Yin, Z. Yin, J. Wang, S. Xu, National assessment of coastal vulnerability to sea-level rise for the Chinese coast, J. Coast Conserv. 16 (2012) 123–133.
[83] K.A. Nguyen, Y.A. Liou, J.P. Terry, Vulnerability of Vietnam to typhoons: a spatial assessment based on hazards, exposure and adaptive capacity, Sci. Total Environ. 682 (2019) 31–46.
[84] M. Xia, K. Jia, W. Zhao, S. Liu, X. Wei, B. Wang, Spatio-temporal changes of ecological vulnerability across the Qinghai-Tibetan Plateau, Ecol. Indic. 123 (2021) 107274.
[85] K.F. Dintwa, G. Letamo, K. Navaneetham, Measuring social vulnerability to natural hazards at the district level in Botswana, Journal of Disaster Risk Studies 11 (1) (2019) 1–11.
[86] A. Getis, J.K. Ord, The analysis of spatial association by use of distance statistics, Geogr. Anal. 24 (3) (1992) 189–206.
[87] M. Ding, Y. Wei, A conceptual framework for quantitatively understanding the impacts of floods/droughts and their management on the catchment's social-ecological system (C-SES), Sci. Total Environ. 828 (2022) 154041.
[88] P. Vedeld, A. Angelsen, J. Bojö, E. Sjaastad, G.K. Berg, Forest environmental incomes and the rural poor, For. Pol. Econ. 9 (7) (2007) 869–879.
[89] D.N. Wear, M.G. Turner, R.O. Flamm, Ecosystem management with multiple owners: landscape dynamics in a southern Appalachian watershed, Ecol. Appl. 6 (4) (1996) 1173–1188.
[90] X. Zeng, Z. Hu, A. Chen, W. Yuan, G. Hou, D. Han, D. Luo, The global decline in the sensitivity of vegetation productivity to precipitation from 2001 to 2018, Glob. Change Biol. 28 (22) (2022) 6823–6833.
[91] J.R. Araújo, A.M. Ramos, P.M. Soares, R. Melo, S.C. Oliveira, R.M. Trigo, Impact of extreme rainfall events on landslide activity in Portugal under climate change scenarios, Landslides 19 (10) (2022) 2279–2293.
[92] H. Jia, X. Wang, W. Sun, X. Mu, P. Gao, G. Zhao, Z. Li, Estimation of soil erosion and evaluation of soil and water conservation benefit in terraces under extreme precipitation, Water 14 (11) (2022) 1675.
[93] P. Marcinkowski, S. Szporak-Wasilewska, I. Kardel, Assessment of soil erosion under long-term projections of climate change in Poland, J. Hydrol. 607 (2022) 127468.
[94] J. Padhiary, K.C. Patra, S.S. Dash, A novel approach to identify the characteristics of drought under future climate change scenario, Water Resour. Manag. 36 (13) (2022) 5163–5189.
[95] H. Etemadi, S.Z. Samadi, M. Sharifikia, J.M. Smoak, Assessment of climate change downscaling and non-stationarity on the spatial pattern of a mangrove ecosystem in an arid coastal region of southern Iran, Theor. Appl. Climatol. 126 (2016) 35–49.
[96] T. Chaudhary, W. Xi, M. Subedi, S. Rideout-Hanzak, H. Su, N.P. Dewez, S. Clarke, East Texas forests show strong resilience to exceptional drought, Forestry 96 (3) (2023) 326–339.
[97] S. Javadinejad, Vulnerability of Water Resources to Climate Change and Human Impact: Scenario Analysis of the Zayandeh Rud River Basin in Iran, University of Birmingham, 2016. Doctoral dissertation.
[98] S. Kamali, K. Asghari, The effect of meteorological and hydrological drought on groundwater storage under climate change scenarios, Water Resour. Manag. 37 (8) (2023) 2925–2943.
[99] A.S. Assani, A.K. Yarou, N.V. Dedehou, H.S. Worogo, M.N. Baco, M. Houinato, I.T. Alkoiret, Towards indigenous community-based adaptation to climate change: a typological analysis of tree-livestock integration in smallholding systems in dryland areas of Benin (West-Africa), Agrofor. Syst. 98 (1) (2024) 197–211.
[100] A.T. Giliam, The Impact of Agroecology Training on the Adaptability of Smallholder Communities to Climate Change in the Mopani District of Limpopo, Stellenbosch University, Stellenbosch, 2018. Doctoral dissertation.